Available online at www.sciencedirect.com

ScienceDirect

Physics Procedia 83 (2016) 706 – 715

Physics Procedia

9th International Conference on Photonic Technologies - LANE 2016

Laser cladding of Ni50Cr: A parametric and dilution study

B. Song[a], T. Hussain[a], K.T. Voisey[a,*]

[a]*Faculty of Engineering, The University of Nottingham, Nottingham NG7 2RD, UK*

Abstract

The increasing use of biomass as a fuel is leading to higher fireside corrosion of the heat exchangers in boilers due to the high chlorine and alkali metal content in the fuel. Laser cladding of Ni50Cr is a promising technique to enhance fireside corrosion resistance of boiler tubes from this aggressive environment. A parametric study is carried out on the blown powder based laser cladding of Ni50Cr on 304 stainless steel. Successful deposits were generated and the effects of the various process parameters on clad geometry and dilution are reported. The various commonly used techniques for determination of clad dilution are compared and some guidelines for their use are suggested.

© 2016 The Authors. Published by Elsevier B.V. This is an open access article under the CC BY-NC-ND license (http://creativecommons.org/licenses/by-nc-nd/4.0/).

Peer-review under responsibility of the Bayerisches Laserzentrum GmbH

Keywords: laser cladding; Ni50Cr; parameter; dilution

1. Introduction

As a result of the move away from fossil fuels there is an increase in the use of biomass fuels. However, the high chlorine and alkali metal (mainly sodium and potassium) contents of biomass fuels can generate severe corrosion problems at high temperatures, > 500 ℃, typical of boilers (Bryers 1991, Michelsen, Frandsen et al. 1998). The high temperature corrosion can be retarded by limiting the steam temperature in superheater tubes to < 450 ℃, as has been done successfully in Denmark (Nielsen, Frandsen et al. 2000), however this is at the expense of decreased boiler efficiency. In order to manufacture biomass fuel-fired boilers with higher efficiency temperatures > 550 ℃) (Michelsen, Frandsen et al. 1998), this fireside corrosion issue must be overcome. Recently, new heat resistant boiler steels grades such as T/P 22, 23, 24, 91 and 92 have been produced for coal-fired ultra super critical (USC) boilers requiring materials with advanced creep properties to obtain steam at severe temperatures and pressures (Vaillant, Vandenberghe et al. 2008). Supercritical (SC) and ultra-supercritical (USC) power plants operate at temperatures

* Corresponding author. Tel.: +44-115-9514139 .
E-mail address: katy.voisey@nottingham.ac.uk

1875-3892 © 2016 The Authors. Published by Elsevier B.V. This is an open access article under the CC BY-NC-ND license (http://creativecommons.org/licenses/by-nc-nd/4.0/).
Peer-review under responsibility of the Bayerisches Laserzentrum GmbH
doi:10.1016/j.phpro.2016.08.072

and pressures above the critical point of water, i.e. above the temperature and pressure at which the liquid and gas phases of water coexist in equilibrium, at which point there is no difference between water gas and liquid water. This results in higher efficiencies – above 45%. Most work on the corrosion resistance of these materials focusses on corrosion in ultra super critical steam medium. The results published in the open literature on their fireside corrosion resistance in fossil fuel boiler environments show acceptable performance (Abang, Lisk et al. 2013). However, such boiler materials may have poor performance when used in biomass boilers due to the unique corrosion and attack mechanism. For instance, the presence of KCl in the deposit formed on boiler grade TP 347H FG stainless steel made the corrosion attack more severe, resulting in the formation of a more uniform and deeper internal attack as the KCl content increased (Lith, Frandsen et al. 2009). Jonsson et al. (Jonsson, Folkeson et al. 2011) showed that the corrosion process of Fe–2.25Cr–1Mo steel was initiated below 400 °C, leading to a fast redistribution of KCl particles and iron ions on the metal surface and reported that chlorine increases the oxidation rate (by decorating oxide grain boundaries) and decreases the oxide scale adhesion.

The use of a suitable corrosion resistant coating is an economically attractive approach to solving this problem. Among available and commercial coating material, NiCr based cermets and alloys are widely used commercially to provide erosion and corrosion resistance even at elevated temperatures. Several major surface techniques have been adopted by industry and researchers. Thermal spraying techniques such as high velocity oxygen fuel (HVOF) (Kim, Hwang et al. 2003, Bhaduri, Indira et al. 2004, Al-Fadhli, Stokes et al. 2006, Sidhu, Sidhu et al. 2006, Oksa, Auerkari et al. 2014) have been used to spray protective coating on surface of boiler tubes and heat-exchangers. Chemical vapour deposition (CVD) (Kalivodova, Baxter et al. 2005) and physical vapour deposition (PVD) (Leyens, Wright et al. 2000) are also utilized to deposit protective coatings for boilers. However, their deposition rate and limitation of heat-exchanger size due to the size of process chamber restrict potential application in boiler industry. Welding techniques such as GTAW (Kawahara 2013) are other kinds of widely used surface technology in boiler coating industry. Innovative techniques in this area include cladding with high energy beams, i.e. plasma and laser cladding. Laser cladding is especially popular due to its well-known advantages of high quality of deposited coating microstructure, small heat affected zone (HAZ), acceptable cost and high deposition speed.

Uusitalo et al. conducted a series of corrosion tests in chlorine containing atmosphere on boiler steels, HVOF thermal sprayed NiCr alloy coatings and laser-melted HVOF NiCr alloy coatings, for 100, 400, and 1000 h (Uusitalo, Vuoristo et al. 2002, Uusitalo, Vuoristo et al. 2003, Uusitalo, Vuoristo et al. 2004). The NiCr alloys used were Ni50Cr and Ni57Cr. The corrosion resistance of these Ni-based, high Cr coating materials was satisfactory in test conditions. Interconnected porosity, oxide-containing splat boundaries, voids formed at splat boundaries and compositional in homogeneities created by HVOF thermal spraying processes limited the corrosion resistance of coatings (Bluni and Marder 1996). Nevertheless, the best HVOF coatings were able to totally protect the coated low-alloy ferritic steel from corrosion attack for short periods, with laser melting remarkably increasing the corrosion resistance of HVOF coatings due to elimination of the original thermally sprayed microstructure. It is therefore expected that a laser clad NiCr layer will provide a better solution to chlorine-associated corrosion than a thermally sprayed coating of the same composition since the laser clad microstructure will be free from included oxides and extensive porosity (Schneider 1998). Previous work of some researchers has shown the potential for laser clad NiCr based alloys as corrosion resistant coating. Li et al. (Li, Li et al. 2013) deposited Hastelloy C22 alloy (Ni-Cr-Mo) on TP347H stainless steel tube and corrosion performance in an HCl environment. Laser clad C22 layer outperformed both the uncoated steel and bulk C22. This superior chlorine corrosion resistance was attributed to the presence of protective Cr_2O_3 in the scale and the refined grain structure typical of laser cladding.

In this study, laser cladding using Ni50Cr alloy powder was performed with various process parameter combinations to deposit single tracks. Cross-sections of the tracks were generated in order to determine track geometry, composition and microstructure. Relationships between input process parameters and clad track characteristics were investigated. Optimal process parameters are identified for manufacture of samples for future high temperature chlorine-associated corrosion tests. In addition, the various commonly used techniques to determine clad dilution are compared and guidelines for their use presented.

Nomenclature

W	width of laser cladding track (mm)
H	height of laser cladding track (mm)
h	melt depth of laser cladding track (mm)
η	dilution ratio of laser cladding track (%)
ρ_c	density of cladded alloy powder (g cm^{-3})
ρ_s	density of substrate material (g cm^{-3})
X_{c+s}	weight percent of element X in the total surface of the clad region (%)
X_c	weight percent of element X in the substrate (%)
A_1	area of the clad region which is above the substate (mm^2)
A_2	area of the clad region which beneath the substate (mm^2)
r_l	radius of the laser beam (mm)
P	Power of the laer beam (kW)
PFR	Powder feed rate (g min^{-1})
v	Laser beam scanning speed (mm min^{-1})
E	Power density (J mm^{-2})
G	Powder density (g mm^{-2})

2. Experimental

2.1. Laser cladding

As shown in Fig. 1, laser cladding is an additive manufacturing technology in which a powdered or wire feedstock material is melted and deposited on a surface via the action of a laser (Toyserkani, Khajepour et al. 2004). The basic principle is quite simple, i.e. rapid melting of the surface layer and coating material, followed by solidification (Desale, Paul et al. 2009). A large variety of operating parameters and physical phenomena determine the quality of laser cladding. The three major input parameters are laser power; powder feed rate and scanning speed of laser beam (Toyserkani, Khajepour et al. 2004). The outputs of the laser cladding process which can be used to determine clad quality are geometry, microstructure and composition. A good clad should be free from defects such as cracks, porosity and coarse grains. Dilution is the change in composition of the clad material due to mixing with the substrate whilst molten. Elements from substrate are usually detrimental to cladded layer's total properties so it is generally required to keep dilution to minimal levels, typically between 5～8 % are regarded as acceptable (Toyserkani, Khajepour et al. 2004).

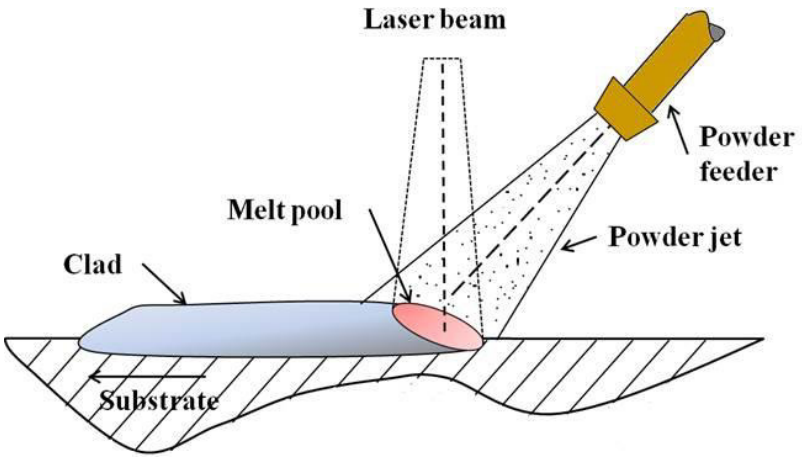

Fig. 1. Schematic of the powder laser cladding process.

2.2. Laser cladding system setup and precautions

The laser cladding system used in this study contains of three main components: a 2 kW IPG (Oxford, UK) Ytterbium-doped, continuous-wave fibre laser operating at a wavelength of 1070 nm coupled with a beam delivery system (125 mm collimating lens and a 200 mm focussing lens), a lateral copper jet nozzle coupled with a powder feeder (Model 1264 manufactured by Miller Thermal Inc. and Praxair Surface Technologies), and a computer numerically controlled (CNC) 4 axis table. The substrate surface was positioned 20 mm below the focal plane, producing a laser spot diameter of 3.1 mm on the surface.

To protect clad tracks from oxidation, the cladding process was performed in an argon filled chamber. The substrate was exposed to an initial laser pass to clean the surface and elevate the substrate temperature to approximately 200 °C before the cladding process began. These surfaces pre-treatment cleaned the surface before deposition.

2.3. Process parameters matrix

All results presented in this paper are from single track, i.e. non-overlapping, clads. Three major parameters were investigated: laser power, powder feed rate and scanning speed, as summarised in Table 1. Two batches of samples were used: In the first batch, laser power was increased from 1 kW to 1.8 kW in 0.2 kW steps; three scanning speeds were used: 200, 250 and 300 mm min^{-1}; powder feed rates were 5, 10, 15 and 20 g min^{-1}. In the second batch, lower laser powers of 0.4, 0.6 and 0.8 kW were used with scanning speeds of 200 and 300 mm min^{-1}; powder feed rate was reduced to 4 and 5 g min^{-1}. This resulted in a total of 37 parameter combinations. Throughout this paper the individual tracks are referred to using the following coding convention: laser power-scanning speed-powder feed rate, i.e. a track deposited at laser power = 1 kW, scanning speed = 200 mm min^{-1} and powder feed rate = 10 g min^{-1}, has a code of 1.0-200-1.

2.4. Feedstock powder and substrates

Plates of 100 mm × 180 mm × 6 mm were machined from AISI 304 austenitic stainless steel. Before cladding these plates were grit blasted and cleaned with acetone to improve substrate surface laser absorptivity and eliminate contaminants, respectively. The additive material is Ni50Cr powder (1260F/Ni-980-1) with a size range of -53 μm / +20 μm, supplied by Praxair Surface Technology Ltd.

As shown in Fig. 2 (a), as-received powder particles have the spherical shape typical of inert gas atomised particles. Some smaller satellite spheres are also seen around larger particles. Cross-sectioning reveals a dendritic solidification pattern (Fig. 2 (b)).

Table 1. Experimental process parameters.

Process parameters	Values
Laser power	0.6, 0.8, 1.0, 1.2, 1.4, 1.6, 1.8 kW
Laser beam scanning speed	200, 250 and 300 mm min^{-1}
Powder feed rate	4, 5, 10, 15 and 20 g min^{-1}
Powder carrier gas flow rate	0.083 L s^{-1}

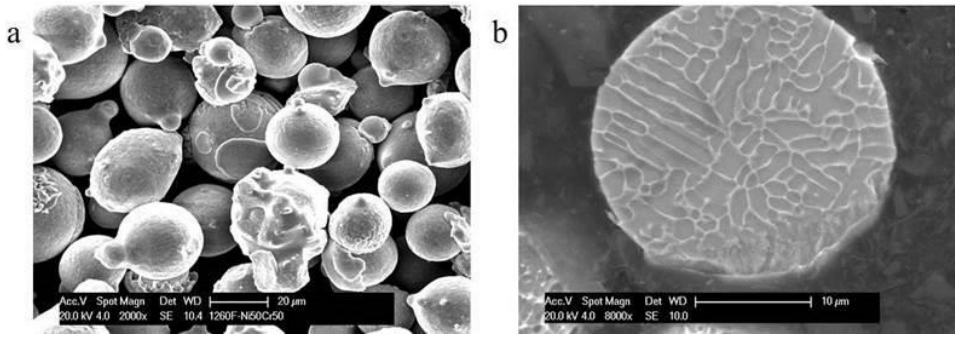

Fig. 2. SEM images of as-received Ni50Cr powder: (a) typical spherical shape of gas atomized powder; (b) dendritic solidification pattern.

2.5. Methods to evaluate laser cladding track quality

To measure geometric features of laser cladding track, width (W), height (H) and melt depth (h) as shown in Fig. 3, track samples were initially transversely sectioned, mounted in conducting resin and sequentially ground and polished using colloidal silica to a 0.6 μm surface finish; then, the track samples were electrolytically etched using 70% orthophosphoric (H_3PO_4) acid in water (typically 6 V for 3 s); after etching, clad bead can be distinguished easily from substrate according to ; finally, values of W, H and h can be measured using ImageJ (National Institute of Health, Maryland, USA) software.

For microstructure analysis, metallographiclly prepared track samples were viewed under a Philips XL 30 Scanning Electron Microscope (SEM) (FEI, Eindhoven, Netherland). Quantitative energy dispersive X-ray analysis (EDXA) (Oxford Instruments, Oxford, UK) was utilised in determining the elemental composition of Fe in the tracks by conducting freehand selection area scan on each cross-sectioned track as the specturm shown in Fig. 3.

Methods of measuring and calculating dilution ratio (η) can be divided into two categories: One is according to the practical test (EDX analysis of Fe content in tracks) of the composition of cladding layer expressed by (Bruck 1988);

$$\eta = \frac{\rho_c \left(X_{c+s} - X_c\right)}{\rho_s \left(X_s - X_{c+s}\right) + \rho_c \left(X_{c+s} - X_c\right)} \tag{1}$$

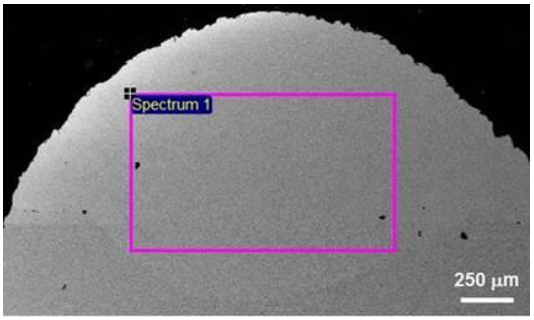

Fig. 3. SEM images of cross section of laser cladding track 1.0-300-10.

The other is based on the measured value of cross-section area of cladding layer. It is called the geometric dilution, which is the simple and general representation of dilution. Exact geometric dilution calculation is indicated in Equation (2) (Bruck 1988). However, for calculation convenience of dilution ratio, the outline of cross-section of cladding layer and the boundary line between cladding material and substrate are both seen as approximated arc, so the areas of Al and A2 can be treated as the section of circle. Then, the expression of dilution ratio can be written as Equation (3) (Zhang, Zhang et al. 2012). Many researchers used more simplified Equation (4), which is simplest and its error need take consideration (Wu, Zhu et al. 1996, Wu, Guo et al. 2015).

$$\eta = \frac{A_2}{A_1 + A_2} \tag{2}$$

$$\eta = \frac{\frac{\left[\left(\frac{W}{2}\right)^2 + h^2\right]^2}{hW}\sin^{-1}\left[\frac{hW}{\left(\frac{W}{2}\right)^2 + h^2}\right] - \left[\left(\frac{W}{2}\right)^2 - h^2\right]}{\frac{h\left[\left(\frac{W}{2}\right)^2 + H^2\right]}{WH^2}\sin^{-1}\left[\frac{\left(\frac{W}{2}\right)^2 + h^2}{\left(\frac{W}{2}\right)^2 + H^2}\right] + \frac{\left(\frac{W}{2}\right)^2 + h^2}{hW}\sin^{-1}\left[\frac{hW}{\left(\frac{W}{2}\right)^2 + h^2}\right] - \frac{\left[\left(\frac{W}{2}\right)^2 - Hh\right](H+h)}{H}} \tag{3}$$

$$\eta = \frac{h}{h + H} \tag{4}$$

In this study, dilution ratio will be measured and calculated using all four kinds of methods (one compositional and three geometrical). Results from all these methods will be compared further to evaluate the accuracy of each method.

3. Results and discussion

3.1. Process window

Visual examination of as-deposited tracks revealed that continuous, adherent tracks had been generated for each parameter combination used. Track widths ranged from 1.7 mm to 4.5 mm and track heights from 0.3 mm to 2.3 mm. The maximum substrate melt depth produced was 0.8 mm. Cross-sections of three different tracks are shown in Fig. 4 in order to illustrate the range of geometries produced.Compositional diluation results ranged from 12 % to 26 %. Fig. 5 summarises the parameter space used in this work. Results are displayed using an arbitrary

definition of a good clad as one with both at least 75% of the interface melted and no porosity. It can be noted that there are no good clads for either extreme of powder feed rate values used: 4 and 20 g/min. It can also be seen that parameter combinations resulting in energy per unit length values of less than 200 kJ/m did not produce any good clads. The area between the two superposed lines is therefore proposed as a suitable process window for laser cladding of Ni50Cr.

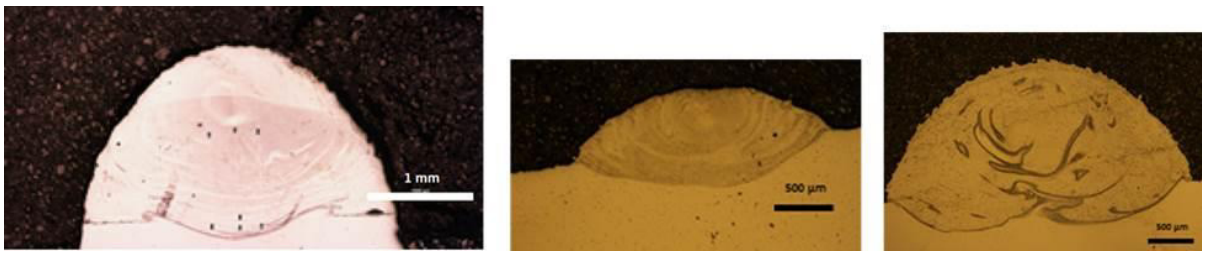

Fig. 4. Optical images of cross sections of laser cladding tracks for the cladding parameters indicated.

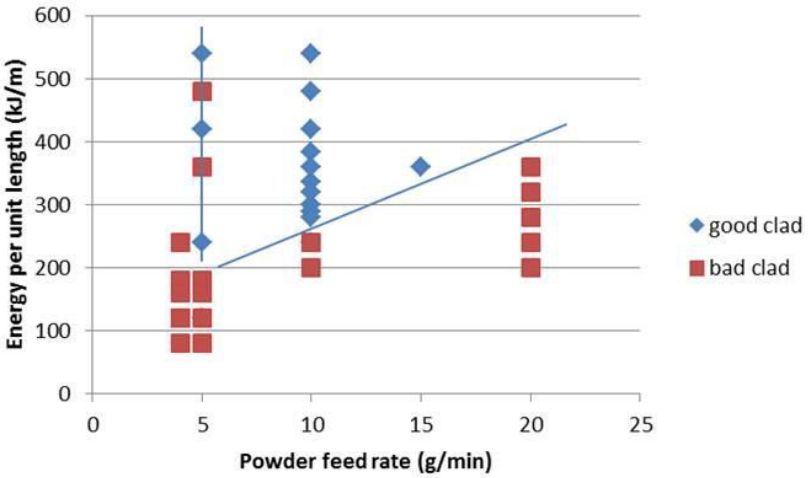

Fig. 5. Variation of clad quality across the parameter space used, the two lines outline the process window.

3.2. Effect of process parameters on clad geometry characteristics and dilution

In Fig.6 the effect of power on aspect ratio and dilution can be seen. Overall the aspect ratio increases with increasing power and decreases with energy per unit length. The dilution increases with both power and energy per unit length. Changing power has a more marked effect on the compositional dilution than on the clad aspect ratio. It should be noted that the 1.4 kW result for 400 kJ/m appears to be an anomaly in both cases. **Fehler! Verweisquelle konnte nicht gefunden werden.** shows results for a powder feed rate of 10 g/min, results for other feed rates showed the same trend of increasing compositional dilution with power and energy per unit length. For all powder feed rates, the effect of power on aspect ratio was less marked than on compositional dilution. An increase in dilution with increasing power is expected due to the increased extent of melting of the substrate that the higher power produces resulting in greater mixing of the substrate and clad material.

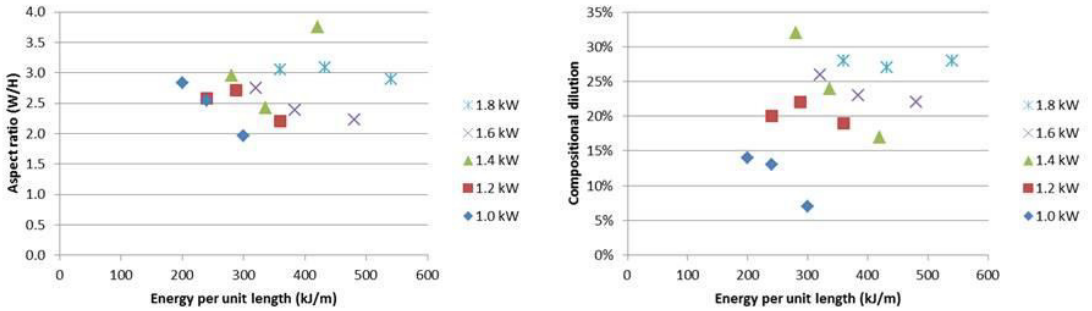

Fig. 6. Effect of laser power on clad track aspect ratio and compositional dilution for clads carried out using a powder feed rate of 10 g/min.

Consideration of the expected effect of power on aspect ratio is less stratightforward as the aspect ratio combines the effects on track width and height. The data used to determine the aspect ratio, the clad track width and height, is therefore plotted directly in Fig. 7 in order to better understand the effect of laser power on clad track dimensions.

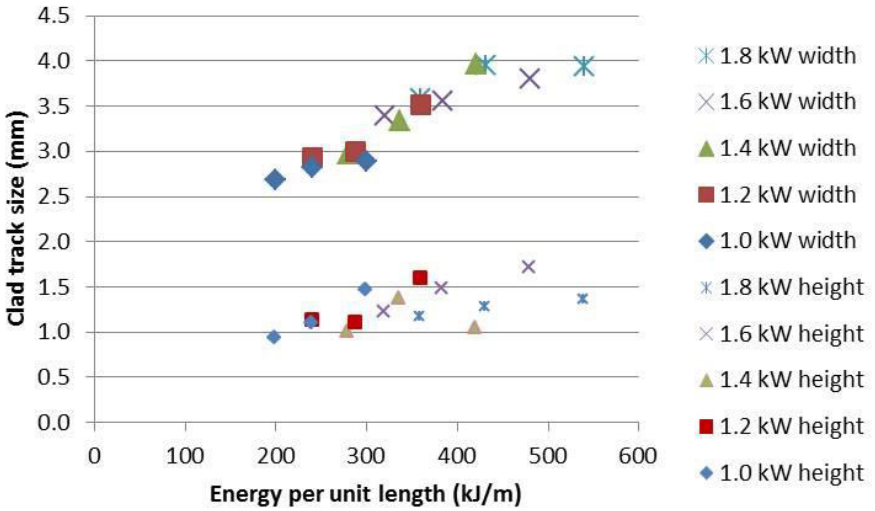

Fig. 7. Effect of power on clad track dimensions for clads carried out using a powder feed rate of 10 g/min.

It can be seen that clad track width increases with increasing energy per unit length. This is expected and is simply due to the larger melt pool that the increased energy input produces. All data points approximately fall on the same straight line, confirming that the key factor influencing the width of clad here is the energy per unit length rather than the laser power. There is greater scatter in the height data, while there is some indication of increasing height with increasing energy per unit length the overall trend is less distinct than for the width data. Looking at the 1.0 kW, 1.6 kW and 1.8 kW height data it can be seen that the gradient of the line through the data points decreases as power increases, suggesting that the influence of energy per unit length decreases as power increases. This may be related to the proportional increase in energy per unit length, however it must be noted that the 1.2 kW and 1.4 kW data do not follow this pattern, hence further investigation of this point is required before any conculsion can be drawn.

3.3. Guidelines for dilution ratio calculation using four methods

Fig. 8 shows dilution ratio results obtained using four different methods. In some cases, such as 1.2-200-5, 1.6-250-10 and 1.6-300-10, results from all four methods are within a few percent of eachother. However there are five cases where the range of the different results exceeds 10%. The 1.0 kW results stand out as a group with a particularly large variation between the compositional dilution and geometric dilution results. There is no significant difference between results obtained using Equation 3 and Equation 4.

Realistic area measurement (Equation 2) usually produces smaller dilution ratios than the methods using Equation 3 and Equation 4. The exception to this is tracks 1.4-200-5, 1.4-200-10, 1.8-200-5 and 1.8-200-10. Clad melted into substrate in those tracks also exhibits a two peak pattern as seen for, 1.4-250-10 in Fig 4.

The potential to obtain different dilution results from different measurement methods has been demonstrated and raises the question of which is the “best” method to use. The answer is that it depends on the application, if clad geometry is a priority then the geometrical dilution methods should be used. If chemical composition is a priority, such as for corrosion work, then an EDS based method should be used, even then thought is required regarding any spatial requirements of composition. Care must also be taken when quoting or comparing dilution results as this can have limited validity if the dilution measurement method is not fully described.

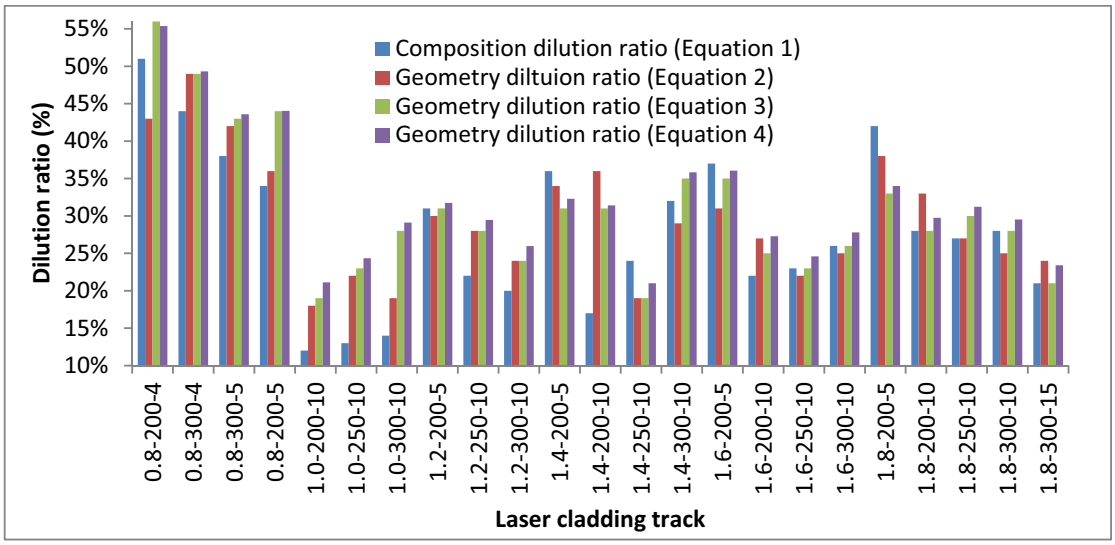

Fig. 8. Comparison of dilution results obtained using different methods.

4. Conclusions

As far as we are aware, this is the first time that laser cladding of Ni50Cr has been demonstrated. Interesting variation in dilution results as a function of measurement technique has been noted. This is likely to be of specific interest to corrosion related applications where corrosion resistance varies with composition, i.e. dilution. Our future work will extend consideration of how best to determine and report dilution. The following specific conclusions can also be drawn:

- Ni50Cr alloy powder was successfully deposited on 304 stainless steel by laser cladding.
- A process window for laser cladding of Ni50Cr has been established.
- Different dilution measurement measurements can produce very different results.

References

Abang, R., A. Lisk and H. J. Krautz (2013). "Fireside corrosion of superheater materials under oxy-coal firing conditions." Energy Procedia 40: 304-311.

Al-Fadhli, H., J. Stokes, M. Hashmi and B. Yilbas (2006). "The erosion–corrosion behaviour of high velocity oxy-fuel (HVOF) thermally sprayed inconel-625 coatings on different metallic surfaces." Surface and Coatings Technology 200(20): 5782-5788.

Bhaduri, A., R. Indira, S. Albert, B. Rao, S. Jain and S. Asokkumar (2004). "Selection of hardfacing material for components of the Indian Prototype Fast Breeder Reactor." Journal of Nuclear materials 334(2): 109-114.

Bluni, S. and A. Marder (1996). "Effects of thermal spray coating composition and microstructure on coating response and substrate protection at high temperatures." Corrosion 52(3): 213-218.

Bruck, G. (1988). Fundamentals and industrial applications of high power laser beam cladding. 1988 Dearborn Symposium, International Society for Optics and Photonics.

Bryers, R. W. (1991). Incinerating municipal and industrial waste.

Desale, G. R., C. Paul, B. Gandhi and S. Jain (2009). "Erosion wear behavior of laser clad surfaces of low carbon austenitic steel." Wear 266(9): 975-987.

Jonsson, T., N. Folkeson, J.-E. Svensson, L.-G. Johansson and M. Halvarsson (2011). "An ESEM in situ investigation of initial stages of the KCl induced high temperature corrosion of a Fe–2.25 Cr–1Mo steel at 400 C." Corrosion Science 53(6): 2233-2246.

Kalivodova, J., D. Baxter, M. Schütze and V. Rohr (2005). "Gaseous corrosion of alloys and novel coatings in simulated environments for coal, waste and biomass boilers." Materials and Corrosion 56(12): 882-889.

Kawahara, Y. (2013). Chapter 10.3 - Application of High-Temperature Corrosion-Resistant Ceramics and Coatings under Aggressive Corrosion Environment in Waste-To-Energy Boilers. Handbook of Advanced Ceramics (Second Edition). S. Somiya. Oxford, Academic Press: 807-836.

Kim, H.-J., S.-Y. Hwang, C.-H. Lee and P. Juvanon (2003). "Assessment of wear performance of flame sprayed and fused Ni-based coatings." Surface and Coatings Technology 172(2): 262-269.

Leyens, C., I. G. Wright and B. A. Pint (2000). "Hot Corrosion of an EB-PVD Thermal-Barrier Coating System at 950°C." Oxidation of Metals 54(5-6): 401-424.

Li, X.-z., H.-c. Li, Y.-t. Wang and B. Li (2013). "Investigations on the behavior of laser cladding Ni–Cr–Mo alloy coating on TP347H stainless steel tube in HCl rich environment." Surface and Coatings Technology 232: 627-639.

Lith, S. C. v., F. J. Frandsen, M. Montgomery, T. Vilhelmsen and S. A. Jensen (2009). "Lab-scale Investigation of Deposit-induced Chlorine Corrosion of Superheater Materials under Simulated Biomass-firing Conditions. Part 1: Exposure at 560° C†." Energy & Fuels 23(7): 3457-3468.

Michelsen, H. P., F. Frandsen, K. Dam-Johansen and O. H. Larsen (1998). "Deposition and high temperature corrosion in a 10 MW straw fired boiler." Fuel Processing Technology 54(1–3): 95-108.

Nielsen, H. P., F. J. Frandsen, K. Dam-Johansen and L. L. Baxter (2000). "The implications of chlorine-associated corrosion on the operation of biomass-fired boilers." Progress in Energy and Combustion Science 26(3): 283-298.

Oksa, M., P. Auerkari, J. Salonen and T. Varis (2014). "Nickel-based HVOF coatings promoting high temperature corrosion resistance of biomass-fired power plant boilers." Fuel Processing Technology 125: 236-245.

Schneider, M. F. (1998). Laser cladding with powder, effect of some machining parameters on clad properties, Universiteit Twente.

Sidhu, H. S., B. S. Sidhu and S. Prakash (2006). "Mechanical and microstructural properties of HVOF sprayed WC–Co and Cr3C2–NiCr coatings on the boiler tube steels using LPG as the fuel gas." Journal of Materials Processing Technology 171(1): 77-82.

Toyserkani, E., A. Khajepour and S. F. Corbin (2004). Laser cladding, CRC press.

Uusitalo, M., P. Vuoristo and T. Mäntylä (2002). "High temperature corrosion of coatings and boiler steels in reducing chlorine-containing atmosphere." Surface and Coatings Technology 161(2): 275-285.

Uusitalo, M., P. Vuoristo and T. Mäntylä (2003). "High temperature corrosion of coatings and boiler steels in oxidizing chlorine-containing atmosphere." Materials Science and Engineering: A 346(1): 168-177.

Uusitalo, M. A., P. M. J. Vuoristo and T. A. Mäntylä (2004). "High temperature corrosion of coatings and boiler steels below chlorine-containing salt deposits." Corrosion Science 46(6): 1311-1331.

Vaillant, J., B. Vandenberghe, B. Hahn, H. Heuser and C. Jochum (2008). "T/P23, 24, 911 and 92: New grades for advanced coal-fired power plants—Properties and experience." International Journal of Pressure Vessels and Piping 85(1): 38-46.

Wu, D., M. Guo, G. Ma and F. Niu (2015). "Dilution characteristics of ultrasonic assisted laser clad yttria-stabilized zirconia coating." Materials Letters 141: 207-209.

Wu, X., B. Zhu, X. Zeng, X. Hu and K. Cui (1996). "Critical state of laser cladding with powder auto-feeding." Surface and Coatings technology 79(1): 200-204.

Zhang, K., X. M. Zhang and W. J. Liu (2012). Influences of processing parameters on dilution ratio of laser cladding layer during laser metal deposition shaping. Advanced Materials Research, Trans Tech Publ.